AIAA JOURNAL
Vol. 40, No. 10, October 2002

Development and Characterization of Hartmann Tube Fluidic Actuators for High-Speed Flow Control

J. Kastner* and M. Samimy†
The Ohio State University, Columbus, Ohio 43210

An in-depth investigation of the Hartmann tube (HT) was carried out to gain a better understanding of and the effects of various parameters on its output flow characteristics. The HT used in this work consisted of an underexpanded jet directed into a close-ended cylindrical tube of the same diameter. The effects of tube depth, separation distance between the tube and the nozzle, and the jet Mach number were explored. Experiments were also performed on an HT fluidic actuator (HTFA). The HTFA operates under the same principles as the HT, except a major portion of the area between the nozzle and tube is shielded off, so that it can be used as a pulsating injector for flow control. Dynamic pressure measurements in the near field and microphone measurements in the far field provided temporal and spectral data. Instantaneous and phase-averaged images of the flow were obtained to explore the nature of turbulence structures within the flow. Limited hot-wire measurements were performed to characterize the velocity fluctuations at the exit of the HTFA. Striking similarities were observed in the frequency content and amplitude of tonal frequencies in near-field pressure and far-field acoustic measurements, as well as the flow results. Time traces of pressure in the tube were used to explain the major differences between the primary frequency of HT and the quarter-wave frequency. Flow visualization results showed a pulsating flow very rich in vortical structures. These images also revealed that the separation distance between the nozzle and the tube has a significant effect on the direction of the pulsating jet out of HT. The results illustrate many similarities, but also some differences between the HT and the HTFA.

Nomenclature

c	=	speed of sound
d	=	nozzle exit diameter and diameter of tube
f	=	frequency
f_{qw}	=	quarter wave frequency
L	=	depth of resonance tube
L_S	=	shock cell length
M_j	=	jet Mach number
Δx	=	separation distance between nozzle and tube

Introduction

Hartmann Tube

A PITOT probe is a simple device that has been used for stagnation pressure measurement since the early days of gasdynamics as an engineering and scientific subject area. It is a tube with one open end that is directly facing the flow and the other end is connected to a pressure gauge and, thus, closed off. If the tube is used in a subsonic flow, the flow isentropically decelerates and reaches zero velocity on a streamline approaching the tube; hence, the stagnation pressure of the flow is measured. If the flow is supersonic, a bow shock is formed in front of the tube, and the measured stagnation pressure is that of the flow after the shock wave, which is lower than the stagnation pressure before the shock wave, due to the highly dissipative nature of the shock wave. When Hartmann and Trolle[1] used a pitot tube in an underexpanded jet in 1927, they obtained an almost sinusoidally varying stagnation pressure along the centerline of the jet, which is expected due to the now well-known compression–expansion pattern in such a flow. However, it was noticed that every time the pitot probe was placed within a compression region of the jet, it resulted in a high-intensity, pure tone noise. Hartmann and Trolle called these regions "intervals of instability." It was later discovered that the tone resulted from the interaction of the jet with the pitot probe.

Once the pitot probe is placed within the compression region of an underexpanded jet, the tube begins to draw fluid in and compression waves are created at the tube entrance (the beginning of compression phase and the overall cycle) that traverse toward the closed end of the tube. The compression waves are reflected by the end wall as compression waves, which move back toward the entrance of the probe. When these waves reach the open end, they are reflected back into the tube as expansion waves (the end of compression phase and the beginning of expansion phase). At this time, the pressure within the tube has risen above the local jet pressure. The tube, therefore, starts relieving itself of the high pressure by ejecting some of the fluid accumulated within the tube. The expansion waves traveling through the tube are reflected on the back wall as expansion waves. Once these waves reach the open end of the tube, they are reflected as compression waves (the end of the expansion phase and the cycle). Once again, the pressure in the tube is sufficiently low to allow the flow of fluid into the tube. Thus, the expansion phase and the overall cycle are complete and the compression phase of the cycle begins again.

The period Δt for this cycle or the frequency f of the cycle can then be calculated from

$$\Delta t = 1/f = L/u_{ci} + L/u_{cr} + L/u_{ei} + L/u_{er} \tag{1}$$

where u is the absolute velocity of the wave (velocity with respect to the tube). For the absolute wave velocity, the first subscript classifies the wave as c for compression and e for expansion, and the second subscript classifies it as i for incident and r for reflected. For accurate calculation of f using Eq. (1), the absolute velocity of the individual waves must be known. An approximate but convenient way to predict the frequency is to assume that all of the waves are Mach waves and, thus, travel with the local speed of sound and to neglect the flow velocity within the tube. With these two assumptions, $u_{ci} = u_{cr} = u_{ei} = u_{er} = c$, and Eq. (1) becomes the quarter-wave frequency equation:

$$\Delta t = 1/f_{qw} = 4L/c \tag{2}$$

Raman et al.[2] have shown that this formula is fairly accurate for long tubes, whereas it overpredicts the frequency for short tubes.

Received 27 October 2001; presented as Paper 2002-0128 at the AIAA 40th Aerospace Sciences Meeting, Reno, NV, 14–17 January 2002; revision received 17 May 2002; accepted for publication 29 May 2002.

*Graduate Student, Department of Mechanical Engineering, Gas Dynamics and Turbulence Laboratory. AIAA Member.

†Professor and Director, Department of Mechanical Engineering, Gas Dynamics and Turbulence Laboratory. Associate Fellow AIAA.

All that has been described so far is what is happening inside the tube. For flow control purposes, the nature of the pulsating jet out of this nozzle-tube system is most relevant. This pulsating jet will follow a cycle in phase with the compression and expansion phases as described. During the compression phase, the pulsating jet will have minimum flow as the air from the nozzle is being compressed into the tube. During the expansion phase, the pulsating jet will have maximum flow as the air from the nozzle is being pushed back by the flow emitting from the tube. The strength of the flow exiting the tube, in comparison with the nozzle flow, will determine the direction of the pulsating jet.

Following Hartmann and Trolle's[1] initial work on the Hartmann tube, much work has been carried out to explore its characteristics. By the use of hydraulic analogy, researchers have been able to better characterize the compression and expansion processes present within the flow.[3–5] Iwamoto and Deckker[3] used the hydraulic analogy to demonstrate the existence of a low-pressure region near the tube entrance. Such a low-pressure region is necessary for oscillations of the flow in Hartmann tubes (HTs).

Brocher et al.[6] described the wave characteristics present within the tube by showing how oscillations within the tube are able to grow or be kept from growing due to a momentum deficit along the jet centerline. This shed light, for example, on why a needle should be used on the axis of an HT with a converging–diverging (C–D) nozzle.[6,7] It has been shown that when the HT with a C–D nozzle is used, it requires a much larger separation distance between the nozzle and the tube in comparison with a HT with converging nozzle.[6,7] This can make an HT with an C–D nozzle somewhat less ideal for an actuator because the larger separation distance would result in a less compact actuator. Raman et al.[7] added a cylindrical shield between the nozzle and tube, covering a large portion of this open surface. This modification converted the HT to a fluidic injector/actuator.

The shape of the HT was changed into a stepped cavity by Sprenger[8] to enhance the heating characteristics of the tube primarily by increasing irreversibilities present within the tube. Kawahashi et al.[9] and Brocher and Ardissone[10] present good summaries of the use of a stepped tube. This alteration of the HT gave way to applications where the end wall was used as a high-frequency pneumatic igniter.[11] Raman et al.[2] tested both a stepped tube and a conical tube. The results showed an increase in frequency from 4 to 6 kHz for a standard cylindrical tube to 7–11 kHz for both the conical and stepped tubes. An amplitude comparison among the three configurations showed variations on the order of 1–3 dB in the amplitude of far-field noise.

Flow Control

It has been known for decades that large coherent structures play major roles in entrainment, mixing, and noise generation in free flows.[12–16] Active control of these structures is an effective and desirable way of manipulating these processes.[15,17–19] The conventional method of low-amplitude forcing at the instability frequencies of the flow has been limited in high-speed flows for two reasons. First, instability frequencies in a typical laboratory flow are very high. For a typical 2.54-cm-diam axisymmetric jet of 400 m/s velocity, the shear layer instability is on the order of 80 kHz, and the jet column frequency is 3–10 kHz. Second, high Reynolds number flows possess high dynamic loading and noisy environment, which require high-amplitude actuators. The lack of the availability of actuators with high bandwidth and high amplitude has been one of the main obstacles in active control of high-speed flows.

Three promising events have taken place in recent years that show the potential of such actuators in high-speed flow control. First, it has been shown that shear layers of a high-Reynolds-number jet can be forced at jet column frequency, but the required forcing amplitude is much higher than that used traditionally.[19] Second, high-Reynolds-number shear layers can also be forced with frequencies much higher than their instability frequencies through the use of higher amplitudes.[20,21] This work was performed in a cavity flow with strong resonance. It remains to be seen whether this can be done in a shear layer with a broadband spectrum. The third event is the recent development of high-bandwidth and amplitude fluidic actuators based on the HT.[2,7] In fact, these actuators have already been used in a cavity flow[20,21] and in an impinging jet.[22]

The frequency characteristics and the effects of various variables such as tube depth, the distance between the nozzle and the tube, and the jet Mach number (or the nozzle pressure ratio) have been explored by many researchers for the HT and by Raman et al.[2] for the actuators based on the HT. However, not much is known on the flow out of either one. This kind of information is important when the fluidic actuator is used for flow control. The main objective of the current work is to provide some information on flow characteristics, along with additional information on other aspects of the actuator.

Experimental Setup

Facility

A modular HT was constructed that allowed for the adjustment of various parameters. Figure 1 shows a schematic of the HT where the tube diameter d, the separation distance Δx, and the tube depth L are all labeled. The diameters of the nozzle and the tube were both equal to 6 mm for all experiments reported here. The tube was constructed with a piston to allow for the depth of the tube to be varied from $1d$ all the way up to $15d$. The piston was sealed in the tube with an O-ring. This setup was designed to provide an approximate frequency range [Eq. (2)] from 1 kHz for $15d$ up to 14 kHz for $1d$. This whole range was not realized experimentally, especially toward the higher-frequency end. As will be discussed later, the maximum amplitude occurs when $\Delta x = 1d$. Because for maximum frequency $L = d$ and because $f \sim L^{-1}$, to achieve higher frequency, one needs to use a nozzle and tube with smaller diameter.

Another parameter that was varied in the current setup was the separation distance between the nozzle and the tube. A Newport linear stage with a micrometer was used to control precisely the separation distance. The setup allowed for the separation distance to be varied between 1 and $3d$. By the variation of the separation distance, the entrance of the tube could be varied with respect to the shock cell structures of the underexpanded jet for a given jet Mach number.

When the HT is used as a fluidic actuator, a cylindrical shield is placed between the nozzle and the tube.[7] This shield directs all of the flow to exit from one side, which allows injection into a flow to be controlled. Such an HT with a shield [HT fluidic actuator (HTFA)] was designed to explore its characteristics and to compare and contrast with those of the HT. A schematic of the current HTFA is shown in Fig. 2. The shield in the current setup is a permanent

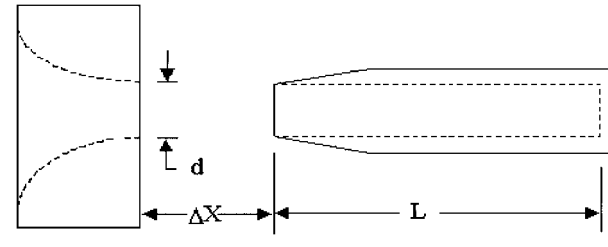

Fig. 1 Schematic of an HT; converging nozzle is on the left and tube on the right.

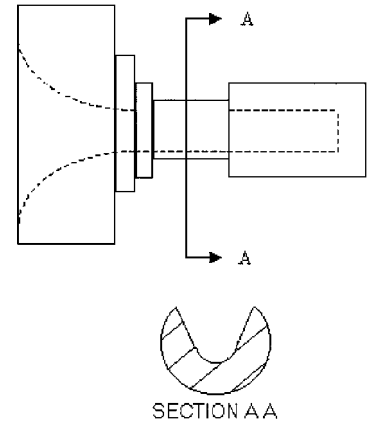

Fig. 2 Schematic of an HTFA.

part of the HTFA. A separation distance Δx of 8 mm between the nozzle and tube was used. Similar to the HT setup, the nozzle and tube diameters were both 6 mm for the HTFA. To vary the depth of the tube for the HTFA, caps were designed that attached directly to the tube. This allowed tube depths of $1d$, $2d$, and $3d$ to be studied. Experiments were performed on the HTFA to explore its characteristics. The results of these experiments, as will be discussed later, showed that the HT and HTFA exhibit similar frequency characteristics. The air supplied to the converging nozzle was controlled by a Grove needle valve (Model 15LH). This setup allowed a pressure ratio up to 5.75 giving a jet Mach number M_j as high as 1.8. A static pressure tap was placed at the exit of the nozzle to determine the jet Mach number.

Acoustic, Pressure, and Velocity Measurements

Far-field acoustic measurements were made 20 jet diameters away from the nozzle exit using a 6.3-mm Bruel and Kjaer (B&K) Model 4135 microphone. The microphone was calibrated with a B&K Model 4231 sound level calibrator. The acoustic signal was low-pass filtered at 80 kHz and a Datel PC416 A/D board was used to sample it at 190 kHz. The data acquisition process was controlled using Labview. Instantaneous near-field pressure data were acquired using a dynamic Endevco pressure transducer (Model 8514-10) attached on the tube 1.2 mm from the open end. The Wheatstone bridge on the pressure transducer was powered with a 10-V excitation provided by an Ectron model 563F signal conditioner. The same signal conditioner was used to amplify the signal before being sent to the Datel PC416 A/D board. The transducers were determined to be accurate up to a frequency of 60 kHz and remained linear within 1–2% of the calibration curve. The signal was low-pass filtered at 60 kHz, and the sampling rate was 190 kHz.

The frequency content of the flowfield between the nozzle and tube was explored using a Uniphase He–Ne continuous wave (cw) laser (Model 106-1). The laser beam of about 1 mm diam was passed through the flowfield, normal to the jet centerline and halfway between the nozzle and tube before reaching a photodiode on the other side. The photodiode measured the intensity of the light and how it varied with time due to the density variations in the flow. This gave a line-of-sight averaged measurement of flow variations affecting the laser beam intensity over the laser path within the flow. As with the microphone and pressure transducer, the data were acquired through Labview using the Datel A/D board.

Velocity measurements using a TSI hot film (Model 1201) were performed on the HTFA to determine its mean velocity, velocity fluctuation level, and frequency content for a typical case. When the hot film was swept through the flowfield, it was found that a location 2 mm before the entrance of the tube and 8 mm perpendicular to the nozzle centerline was a dynamic location. This location was used for velocity measurements. The frequency response of the hot film was determined to be up to 8 kHz. The velocity measurements were performed on an HTFA with an M_j of 1.08 and a tube depth of 18 mm, which had a primary frequency of 3.5 kHz.

Once all of the data were acquired and saved, frequency spectra of the microphone, pressure transducer, photodiode, and hot-film signals were obtained using 8192 data points. The spectra were averaged over 100 data blocks. The sound pressure level was computed for the microphone, whereas the amplitude for the pressure transducer and photodiode were normalized by the corresponding rms value of the signal for $L = 1d$ and $\Delta x = 1d$ case, where the signal had the highest amplitude.

Flow Visualization

Flow visualization was performed using laser sheet illumination. The laser beam was provided from a Continuum Powerlite 8010 Nd : YAG operating at a wavelength of 532 nm. The maximum repetition rate of the laser was 10 Hz, and the pulse duration was 9 ns. With this repetition rate, the laser could not provide time-correlated images. Instead, the laser was phase locked with the far-field acoustic signal of the HT. As will be discussed later, this far-field signal had a distinct primary frequency when the entrance of the HT tube was within a compression region. To obtain phase-locked images, a real-time signal from a B&K microphone was sent to a PC-T10-10 timing board after it was low and high pass filtered to obtain a smoothly varying signal. The filtering allowed for the removal of any harmonics that could interrupt the triggering process. The signal was amplified to have magnitudes recognized by the timing board. The timing program was triggered by the rising edge of the signal once it was greater than 5 V. Once the triggering had taken place, a TTL signal was sent to the laser that was also synchonized with a digital camera.

The laser was used to form a sheet that contained the centerline of the jet/tube of the HT and the HTFA to visualize a part of the jet and flow out of the HT and HTFA. The tube and nozzle were painted black or anodized to reduce scattering of the laser light from the solid surfaces. The laser was synched to a 14-bit Princeton Instruments intensified charge-coupled device camera with a resolution of 588 by 384 pixels through a Princeton Instruments PG-200 programmable pulse generator. The camera was placed orthogonal to the plane of the laser sheet. An extension tube was placed between the camera and the lens to allow zooming of the camera.

Seeding of the flow was accomplished using acetone injected approximately 11 m upstream of the nozzle exit. This long distance was sufficient to allow acetone to evaporate and mix with air before entering the nozzle. After acetone injection, the flow was passed through a chamber to achieve better mixing between the flow and acetone. The flow visualization technique relies on Mie scattering of laser light by acetone particles condensed during flow expansion within the nozzle. For each case, 60 instantaneous images were taken during 8 equally spaced phases of 1 cycle of the primary frequency. These 60 images were used to obtain phase-averaged images.

Results and Discussion

Tube Depth

The depth of the tube has multiple impacts on the results of the HT. Hartmann[23] showed that both the frequency and amplitude peaked around a tube depth of $1d$. The effects of tube depth will be presented and discussed in detail. First, the quarter-wave frequency [Eq. (2)] will be compared with the experimental results, and then the reasons for the observed differences will be discussed in the context of the near-field pressure time traces. The time traces give a good description of the differences between the compression and expansion phases. Finally, the impact of tube depth on amplitude will be briefly explored.

Figure 3 shows the magnitude of the primary far-field acoustic frequency of the HT vs M_j for various tube depths L and the nozzle-tube separation distance Δx. As will be discussed later, the tonal frequency contents of the far-field acoustic and near-field pressure are identical. The quarter-wave frequency f_{qw} for each tube depth is also shown. It is clear from Fig. 3 that, as the tube depth is increased, the frequency is getting closer to the quarter-wave value. This trend is in agreement with the results available in the literature.[2] Table 1 further supports this by showing the minimum and maximum measured frequencies in comparison with the quarter-wave frequency for each tube depth. For a tube depth of $1d$, the actual frequency differs from the quarter-wave frequency by 35–49%, whereas for a tube depth of $6d$, the difference is only from 8 to 17%.

To help understand the reason for these differences, it is beneficial to look at the time trace of pressure in the tube over one cycle. A time

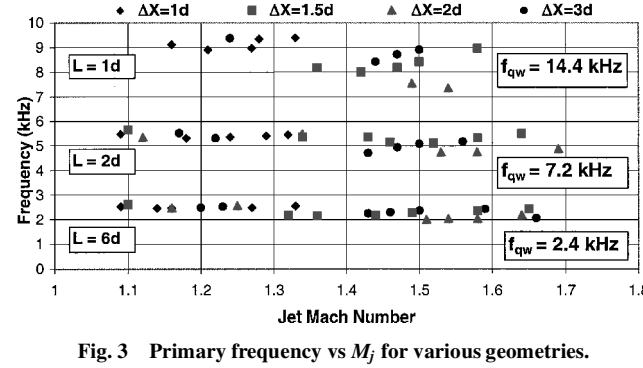

Fig. 3 Primary frequency vs M_j for various geometries.

Table 1 Fundamental and quarter-wave frequencies and percentage duration of compression and expansion phases in a cycle for various tube depth

	Tube depth L			
Parameter	$1d$	$2d$	$3d$	$6d$
Quarter-wave frequency, kHz	14.4	7.2	4.8	2.4
Minimum frequency, kHz	7.4	4.7	3.2	2.0
% Difference	49%	35%	33%	17%
Maximum frequency, kHz	9.4	5.6	4.1	2.6
% Difference	35%	22%	15%	8%
% Time in compression	52%	59%	61%	64%
% Time in expansion	48%	41%	39%	36%

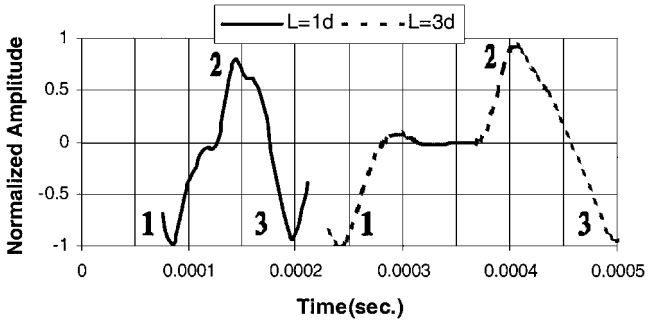

Fig. 4 Time traces of pressure in the tube for two tube depths; $\Delta x = 1d$, $M_j = 1.1$, and $M_j = 1.2$ for shorter and longer tubes.

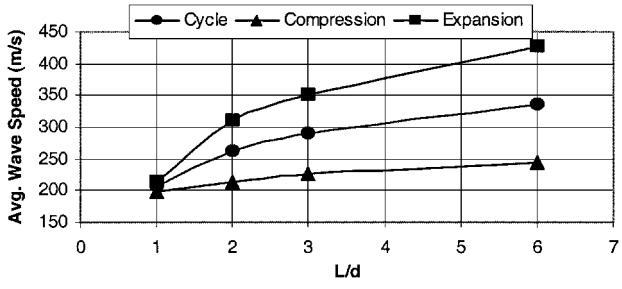

Fig. 5 Average absolute wave speed for compression, expansion, and the cycle for various tube depths.

trace can be used to show the difference between the compression and expansion phases of the HT. Brocher et al.[6] examined the effect of jet Mach number on such a time trace. Figure 4 shows a time trace of the pressure, normalized by the magnitude of negative peak for each case, for two tube depths, $L = 1$ and $3d$. For both time traces, the trough to peak (1–2) represents the compression phase, whereas the expansion phase is occurring during the peak to trough (2–3). For the smaller tube depth, the duration for the compression and expansion phases is approximately the same. On the other hand, for the longer tube depth, the compression phase takes much longer than the expansion phase. The result of this is that the HT is generating a nearly sinusoidal near-field pressure when the tube depth is on the order of $1d$. Table 1 shows the percentage of duration for the compression and expansion phases in a cycle for various tube depths. The compression phase increases from 52% of the cycle for $1d$ all of the way to 64% for $6d$.

The phase information from Fig. 4 and the tube depth were used to calculate the average absolute velocities for compression and expansion phases. Figure 5 shows these velocities along with the average absolute wave speed over the entire cycle for various tube depths. The average compression wave speed was calculated from the time it takes the pressure to rise from trough to peak, and the average expansion wave speed was found from the time taken to go from peak to trough. The average wave speed for the expansion wave is nearly the same as the compression wave for tube depths of $1d$. However, as the tube depth is increased, the expansion wave speed increases faster than the compression wave speed. One noticeable result is that the average absolute wave speed for the cycle is much lower than the speed of sound for the $1d$ case but approaches the speed of sound for larger tube depths.

The results presented in Figs. 4 and 5 provide some clues for the differences between the measured primary and the quarter-wave frequencies that are given in Table 1. The quarter-wave frequency assumes that the waves within the tube in both compression and expansion phases are simple, that is, spatially compact, acoustic or weak waves and neglects flow velocity within the tube. In reality, the waves in part of the compression phase can be assumed to be simple, but this is not the case for the expansion phase. The presence of a plateau in the compression phase in Fig. 4 for the longer tube and the lack of it in the expansion phase confirm this statement. Also, expansion waves will be acoustic waves, but the compression waves will have a speed higher than acoustic waves and only will approach the speed of sound as they become weaker. Therefore, the time for the compression phase must be smaller or equal to that of the expansion phase. However, the results presented in Fig. 4 for the deeper tube shows a longer compression phase, which highlights the effect of flow velocity. Both the expansion and compression waves traveling from the entrance of the tube toward the closed end of the tube encounter quiescent flow within the tube. However, in the return, the expansion waves ride on the flow, which is traveling in the same direction, whereas compression waves and the flow travel in the opposite directions. Sarohia and Back[24] demonstrated that the reflected compression wave was slowed down as a result of the flow velocity within the tube.

In addition to its effect on the frequency, the tube depth affects the amplitude of the primary frequency peak for both the far-field acoustic and the near-field pressure. It was observed that, as the tube depth is increased or the frequency is decreased, the amplitude of the primary frequency peak is decreased as well. The reduction in amplitude is nonlinear and appears to be leveling off toward the lower frequencies: Changing the tube depth between 1 and $2d$ has a more drastic effect than changing it between 3 and $6d$. The current results, which show that the amplitude is maximum at $L = 1d$, is in agreement with previous results.[23,25]

Jet Mach Number/Nozzle Pressure Ratio

In the current configuration, which uses a converging nozzle, the tonal frequencies appear only when the jet is operated in the underexpanded flow regime and the tube entrance is in a compression region of the jet. The exit pressure of the nozzle is higher than the ambient pressure for this flow regime. The degree of underexpansion can be expressed by either the ratio of stagnation pressure to ambient pressure or jet Mach number, which is obtained by a hypothetical isentropic expansion of the flow from the given stagnation pressure to the ambient pressure. The latter is chosen here. Figures 6 and 7 show frequency spectra of acoustic and pressure signals for two cases with similar geometry (the tube depth and the separation distance of $1d$) but with different jet Mach numbers ($M_j = 1.16$ and 1.33). Two main observations are the striking similarity of the tonal frequency content of pressure and far-field acoustic signals and the strengthening of the primary peak along with the appearance of more harmonics for the higher jet Mach number M_j case. The stronger compression and expansion waves of the underexpanded jet at higher jet Mach number M_j could lead to stronger compression and expansion waves within the tube. However, this could also be due to relative location of the entrance of the tube within the compression region because the compression/expansion pattern shifts with jet Mach number M_j for a fixed geometry. Norum and Seiner[26] presented the compression cell length L_S as a function of jet Mach number M_j and nozzle diameter d for an underexpanded converging nozzle as

$$L_S = 1.1d\sqrt{M_j^2 - 1} \tag{3}$$

Therefore, in Fig. 6a with a low jet Mach number of 1.16, the compression cell spacing would be around 3.5 mm whereas in Fig. 6b, with the jet Mach number increased to 1.33, the compression cell spacing is around 5.8 mm.

Another experiment was carried out to obtain the frequency content of the flow more locally (averaged over a line), rather than

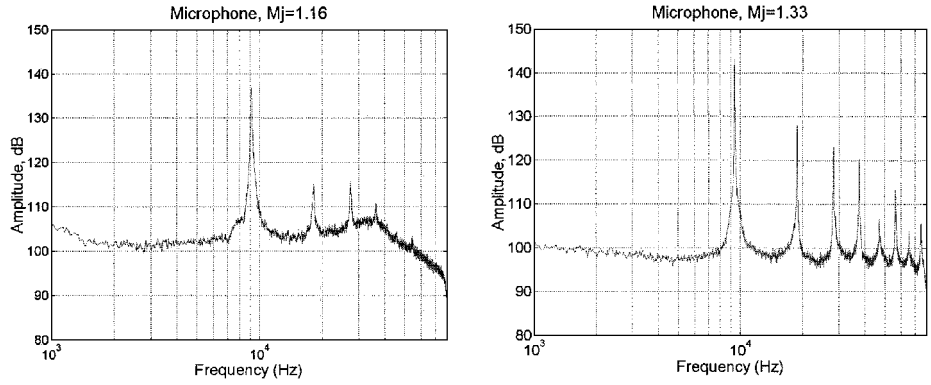

a) b)

Fig. 6 Frequency spectra of far-field acoustic signal for two jet Mach numbers at a fixed geometry of $L = 1d$ and $\Delta x = 1d$.

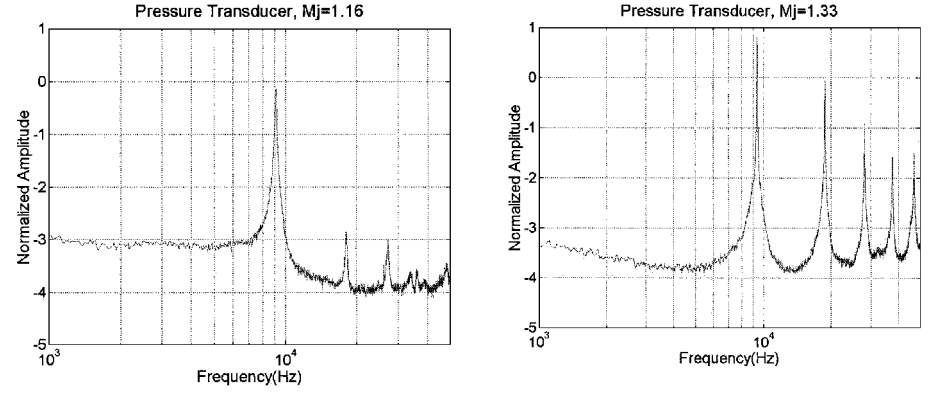

a) b)

Fig. 7 Frequency spectra of near-field pressure signal for two jet Mach numbers with same geometry as in Fig. 6.

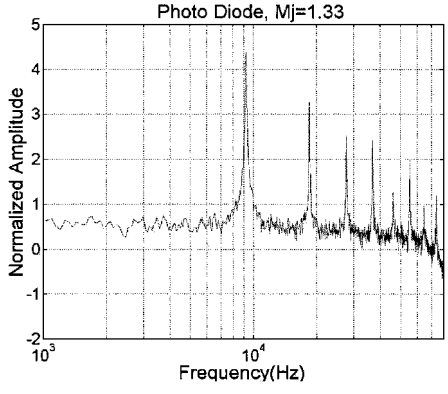

Fig. 8 Frequency spectrum of flowfield for $L = 1d$, $\Delta x = 1d$, and $M_j = 1.33$.

globally, such as that of pressure or acoustic. The beam of a He–Ne laser was passed through the flow before striking the surface of a photodetector. Figure 8 shows the frequency spectrum of the density fluctuations for $L = \Delta x = 1d$ and $M_j = 1.33$. The laser beam was normal to the jet centerline and intersected it 3 mm downstream of the nozzle, halfway between the nozzle and tube. The similarity of the frequency content in the flow (Fig. 8), far-field acoustic (Fig. 6b), and pressure (Fig. 7b) is striking. The He–Ne laser beam was traversed along the jet centerline of the HT looking for any dependence on measurement location. Only the amplitudes of the tonal features were altered with beam location, whereas the frequency content remained nearly unchanged.

Separation Distance

It was discussed earlier that the separation distance between the nozzle and tube has significant influence on the amplitude of primary oscillations, with $\Delta x = 1d$ providing the largest amplitude.

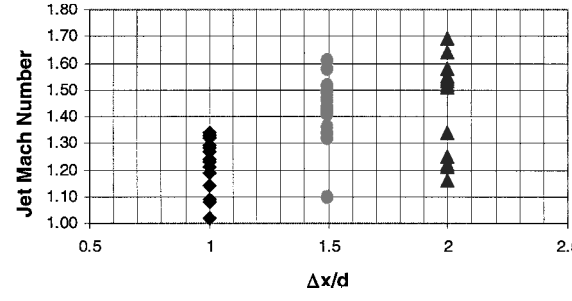

Fig. 9 Variation of required M_j for strong oscilations for various Δx.

Figure 9 shows the range of required jet Mach numbers to achieve a far-field acoustic of above 130 dB at the primary frequency. The separation distance is plotted on the x axis, and each separation distance contains a series of jet Mach numbers for which strong oscillations were observed. The jet Mach number was varied between 1 and 1.8. It is clear from Fig. 9 that as the separation distance is increased the required minimum jet Mach number M_j as well as the range of jet Mach numbers M_j for oscillations to occur is increased. Raman et al.[2] showed similar results for cylindrical, conical, and stepped tubes. These effects stem from the increase in the compression cell length as jet Mach number M_j is increased [Eq. (3)]. Increased operation range, which gives more flexibility, is obviously positive. However, increased minimum jet Mach number M_j is negative because it increases the required mass flow rate in practical applications.

Flow Visualization

Flow visualization was used to gain a better understanding of the flowfield of the HT. If the HT is to be used as a fluidic actuator, it is crucial to understand its flow characteristics. Most researchers in the past have used schlieren or shadowgraph to study the flow of the HT.[3,5,27–29] These techniques provide line-of-sight averaged images.

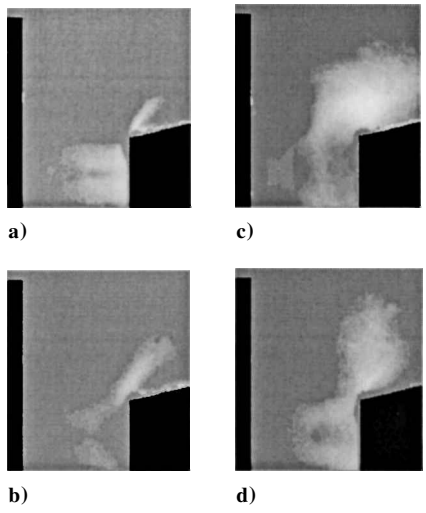

Fig. 10 Phase-averaged flow images for $L = 3d$, $\Delta x = 2d$, and $M_j = 1.6$: a) and b) compression phase and c) and d) expansion phase.

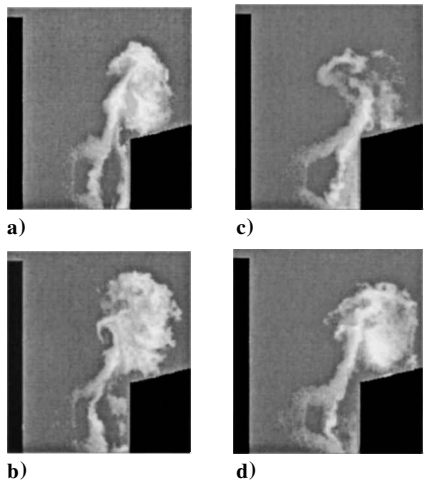

Fig. 11 Instantaneous images for the case in Fig. 10d.

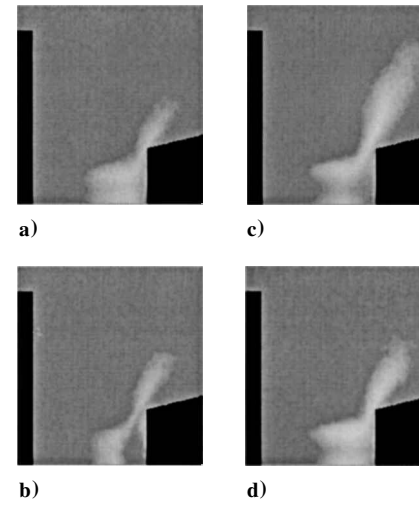

Fig. 12 Phase-averaged flow images for $L = 3d$, $\Delta x = 2d$, and $M_j = 1.3$: a) and b) compression phase and c) and d) expansion phase.

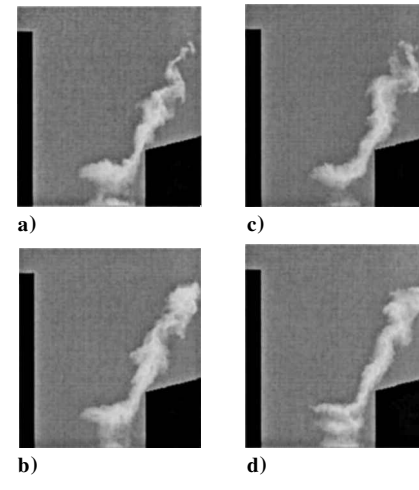

Fig. 13 Instantaneous images for the case in Fig. 12c.

Such images have provided useful information in nominally two-dimensional flows that are not highly turbulent. However, the HT flow is expected to be quite three dimensional and highly turbulent. Therefore, the planar flow visualization technique with a very short exposure time of 9 ns is better suited for this flow.

Figure 10 shows a set of phase-averaged images at four equally spaced phases for a tube depth of $3d$, a separation distance of $2d$, and an M_j of 1.6. The nozzle is barely visible on the left, and the tube is on the right in all of the images. Only the upper-half of the flow is visualized. The mid-compression and expansion phases are shown in Figs. 10a and 10c, respectively. The images are equally spaced in time, 55 μs apart, throughout one cycle. During the expansion phase (Figs. 10c and 10d), the flow out of the HT system is more inclined toward the tube, rather than 90 deg to the centerline of the nozzle/tube. Another characteristic of the flow is that in the compression phase (Figs. 10a and 10b), not all of the jet fluid is being entrained into the tube.

Figure 11 shows four instantaneous images, out of 60 used to get the phase-averaged image of Fig. 10d. Two main observations are that the flow out of the HT in the expansion phase contains coherent structures of various kind and that the phase-averaged images are deceptive.

To explore the effects of M_j, the flow visualization results for the same geometry of Fig. 10 but operating at an M_j of 1.3 are shown in Fig. 12. This case has approximately 40% less mass flux than the earlier one. When Figs. 10a and 10b and 12a and 12b are compared, not much difference can be seen between the two flowfields for the compression phase. During the expansion phase, however, the images for the larger mass flow case show more fluid being ejected, as expected. Comparison of instantaneous images (Figs. 11 and 13) does not reveal any major changes in the flow direction, and both contain organized turbulence structures.

The importance of the separation distance between the nozzle and the tube was discussed earlier. To explore this effect on the flow characteristics, the tube depth and jet Mach number M_j were held fixed at $3d$ and 1.3 as in Figs. 12 and 13, but the separation distance was decreased from $2d$ to $1d$. The phase-averaged images for this case are shown in Fig. 14, and four instantaneous images are shown in Fig. 15. Recall that this is optimum separation distance for pressure and far-field acoustic fluctuations. Three main differences can be seen between the images for the 1 and $2d$ cases, all of which are consistent with the pressure and acoustic results. First, the nozzle flow is pushed back farther for $1d$ case and the exiting jet has an angle of about 90 deg to the nozzle/tube centerline during the expansion phase. Second, more fluid is entrained into the tube, during the compression phase. Finally, the exiting jet contains larger undulations, indicating the presence of more coherent turbulence structures.

Varying the tube depth was already shown to have a major impact on the primary frequency (Fig. 3) and also on the percent of time spent in the compression phase (Fig. 4 and Table 1). When the tube depth was varied, the flows for 1 and $3d$ tube depths did not show any major differences. This is consistent with the schlieren flow visualization results of Thompson.[29]

Flow visualization was also performed on a HTFA configuration to better understand how adding a cylindrical shield between the nozzle and tube would affect the flowfield generated by the HT. The experiments were performed at two separate jet Mach numbers M_j for three tube depths of 1, 2, and $3d$. The separation distance was held constant at 8 mm for all of the images. In all of the images, the

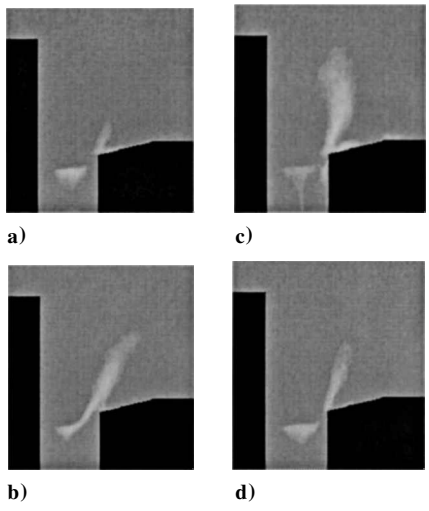

Fig. 14 Phase-averaged flow images for $L = 3d$, $\triangle x = 1d$, and $M_j = 1.3$: a) and b) compression phase and c) and d) expansion phase.

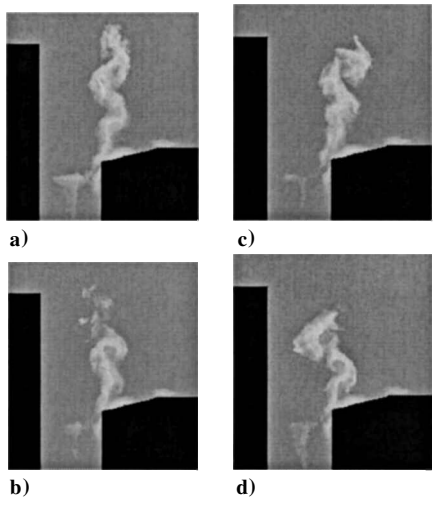

Fig. 15 Instantaneous images for the case in Fig. 14c.

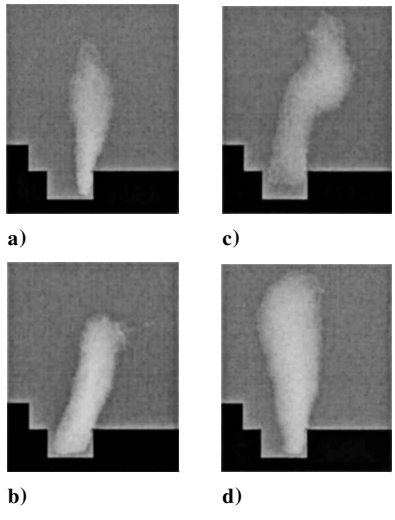

Fig. 16 Phase-averaged flow images for HTFA for $L = 3d$ and $M_j = 1.3$: a) and b) compression phase and c) and d) expansion phase.

nozzle is on the left, the tube is on the right, and the shield is on the lower part of the images extending between the nozzle and the tube. The visualized area covers mostly the pulsating jet out of the HTFA.

Figures 16 and 17 both present phase-averaged and instantaneous images for a tube depth of $3d$ and an M_j of 1.3. The time separation for all $3d$ tube depth images is 70 μs. As expected, the compression phase (Figs. 16a and 16b) shows that not all of the fluid is being

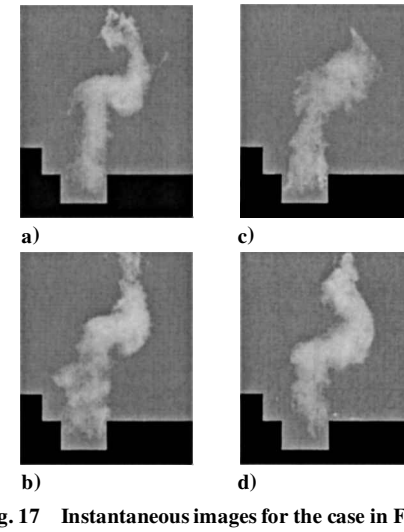

Fig. 17 Instantaneous images for the case in Fig 16c.

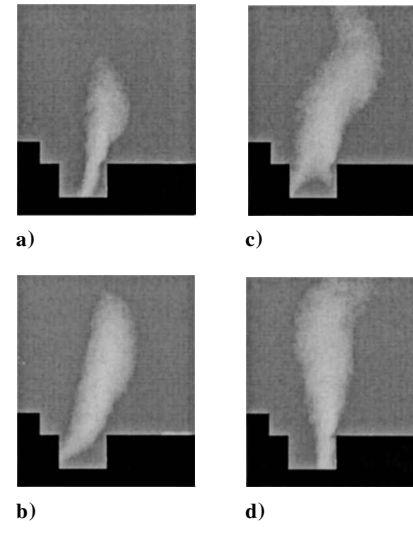

Fig. 18 Phase-averaged flow images for HTFA for $L = 2d$ and $M_j = 1.3$: a) and d) compression phase and b) and c) expansion phase.

entrained into the tube. The mid-expansion phase (Fig. 16c) shows fluid being ejected into the ambient at 90 deg to the jet centerline near the injector, but as the flow moves farther away, it begins to have a wavy appearance. The instantaneous images in Fig. 17 also show this wavy appearance in the expansion phase, which seems to indicate the presence of strong vortical structures in the flow. The undulation shown on the phase-averaged image (Fig. 16a) in the expansion phase was not noticed in any of the phase-averaged images from the HT. Therefore, it either indicates the presence of strong and semi-spatially stationary vortical structures or it is a result of adding the shield. If it is due to the geometry, whether it is specific to this geometry or it is a general characteristic of HTFA is not clear at this time. The images for the same geometry but an M_j of 1.1 show similar characteristics, except for the effect of reduced mass flux that was discussed earlier for the HT.

Figures 18 and 19 present phase-averaged and instantaneous images for a tube depth of $2d$ and an M_j of 1.3. The time separation for all $2d$ tube depth images is 55 μs. Again, the expansion phase has more fluid being ejected for the $3d$ case than the tube with $2d$ case because the tube with a depth of $3d$ can entrain more fluid than the tube with a depth of $2d$.

The HT and the HTFA operate under similar principles. However, when the shield is added, the pulsating flow is concentrated in a smaller area, becomes more voluminous in the images, and possesses higher velocities. The flow for the HTFA during the expansion phase was always being ejected at an angle of 90 deg with respect to the jet centerline, which seems to be due to the proximity of the nozzle and tube because the HT had a pulsating jet at 90 deg only when the separation distance was $1d$. Another noticeable

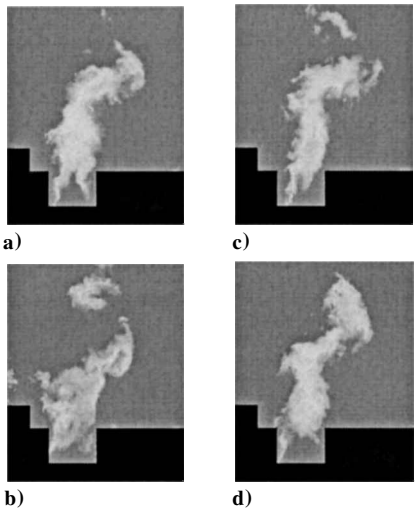

Fig. 19 Instantaneous images for Fig. 18c.

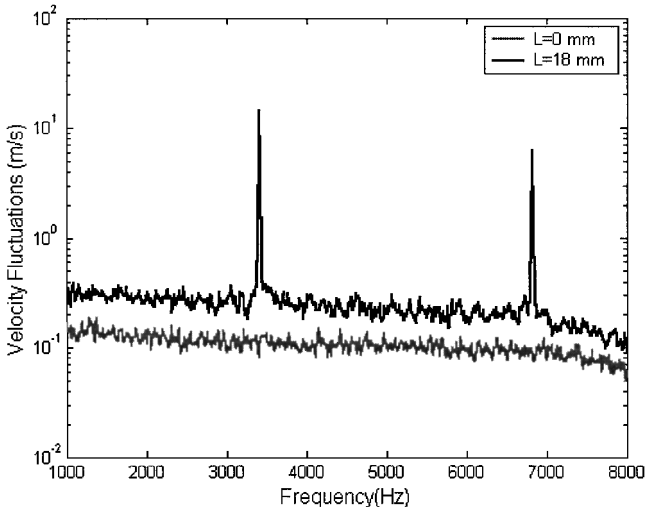

Fig. 20 Comparison of velocity frequency spectra at the exit of a HTFA for a tube depth of 18 mm and a plugged tube; depth = 0 mm.

difference was the presence an undulation in the phase-averaged flow for all the HTFA cases but none for any of the HT cases, the reason for which is not clear at this time.

Velocity Measurements

Velocity measurements were performed on the output flow of a HTFA to characterize its velocity level. Such information is important when HTFA is used as an injector. A HTFA with a 4-mm nozzle exit diameter was used for this purpose and measurements were performed at a location 2 mm before the entrance of the tube and 8 mm perpendicular to the nozzle centerline. Figure 20 presents velocity frequency spectra for two cases: one with a tube depth of 18 mm and one with a plugged tube (0-mm tube depth) and, thus, eliminating pulsating jet and tonal frequencies. The HTFA with a tube depth of 18 mm has significantly higher velocity fluctuations when compared to the plugged-tube case. It also includes two strong tonal frequencies. The mean velocity for the plugged-tube case was 170 m/s, and the turbulence intensity was 2.5%, whereas for a tube depth of 18 mm, the mean was reduced to 140 m/s, and the velocity fluctuation intensity was increased to 18%. Also in Fig. 20, for the tube depth of 18 mm, the tonal frequency was approximately 3.5 kHz, which falls within the band of frequencies measured at a similar tube depth for the stand-alone HT configuration (Table 1).

Conclusions

A modular HT was constructed to examine the effect of various geometric and flow parameters on its characteristics. The parameters included tube depth, separation distance, and the jet Mach number. Dynamic pressure measurements in the near field and microphone measurements in the far field provided both temporal and spectral data. Instantaneous and phase-averaged images of the flow allowed exploration into the nature of the flow exiting the HT.

The near-field pressure, far-field acoustic, and flow results yielded similarities in both the frequency content and amplitude of the tonal frequency. Time traces of the pressure on the tube wall provided insight into the major differences between the primary frequency of the HT and the predicted quarter-wave frequency. Flow visualization results displayed a highly pulsating flow, which was very rich in vortical structures. They also showed the significant effect that the separation distance has on the direction of the pulsating jet out of HT, which would play a major role in flow control. Flow visualizations were also taken of an HTFA. The flow from the HTFA was much more concentrated due to the addition of a shield between the nozzle and the tube. The flow results illustrate many similarities, but also some differences between HT and HTFA.

Acknowledgments

The initial support of this research by an Air Force Office of Scientific Research AASERT grant (with T. Beutner) and its current support by a DAGSI grant (with AFRL/VA, M. Stanek) are both greatly appreciated. Jason Petric, an undergraduate student, whose contribution is very much appreciated, carried out part of the Hartmann tube fluidic actuator experimental work. The help of James Hileman and Brian Thurow both in the experimental phase of this work and for editing the manuscript and also the help of Marco Debiasi for editing the manuscript are all greatly appreciated.

References

[1]Hartmann, J., and Trolle, B., "A New Acoustic Generator," *Journal of Scientific Instruments*, Vol. 4, No. 4, 1927, pp. 101–111.

[2]Raman, G., Mills, A., Othman, S., and Kibens, V., "Development of Powered Resonance Tube Actuators for Active Flow Control," American Society of Mechanical Engineers, Paper ASME FEDSM 2001-18273, 2001.

[3]Iwamoto, J., and Deckker, B. E. L., "A Study of the Hartmann-Sprenger Tube Using the Hydraulic Analogy," *Experiments in Fluids*, Vol. 3, No. 5, 1985, pp. 245–252.

[4]Morch, K. A., "A Theory for the Mode of Operation of the Hartmann Air Jet Generator," *Journal of Fluid Mechanics*, Vol. 20, Pt. 1, 1964, pp. 141–159.

[5]Solomon, L., "Hydraulic Analogue Study of the Hartmann Oscillator Phenomenon," *Journal of Fluid Mechanics*, Vol. 28, Pt. 2, 1967, pp. 261–271.

[6]Brocher, E., Maresca, C., and Bournay, M.-H., "Fluid Dynamics of the Resonance Tube," *Journal of Fluid Mechanics*, Vol. 43, Pt. 2, 1970, pp. 369–384.

[7]Raman, G., Kibens, V., Cain, A., and Lepicovsky, J., "Advanced Actuator Concepts for Active Aeroacoustic Control," AIAA Paper 2000-1930, 2000.

[8]Sprenger, H., "Ueber thermische Effekte in Resonanzrohen," Vol. 21, Federal Inst. of Technology, Zurich, 1954, pp. 18–35.

[9]Kawahashi, M., Bobone, R., and Brocher, E., "Oscillation Modes in Single-Step Hartmann-Sprenger Tubes," *Journal of the Acoustical Society of America*, Vol. 75, No. 3, 1984, pp. 780–784.

[10]Brocher, E., and Ardissone, J-P., "Heating Characteristics of a New Type of Hartmann–Sprenger Tube," *International Journal of Heat and Fluid Flow*, Vol. 4, No. 2, 1983, pp. 97–102.

[11]Marchese, V. P., Rakowsky, E. L., and Bement, L. J., "A Fluidic Sounding Rocket Motor Ignition System," *Journal of Spacecraft and Rockets*, Vol. 10, No. 11, 1973, pp. 731–734.

[12]Brown, G. L., and Roshko, A., "On Density Effects and Large Structure in Turbulent Mixing Layers," *Journal of Fluid Mechanics*, Vol. 64, 1974, pp. 715–816.

[13]Crow, S. C., and Champagne, F. H., "Orderly Structure in Jet Turbulence," *Journal of Fluid Mechanics*, Vol. 48, 1971, pp. 547–591.

[14]Ho, C.-M., and Huang, L.-S., "Subharmonics and Vortex Merging in Mixing Layers," *Journal of Fluid Mechanics*, Vol. 119, 1982, pp. 443–473.

[15]Kibens, V., "Discrete Noise Spectrum Generated by an Acoustically Excited Jet," *AIAA Journal*, Vol. 18, No. 4, 1980, pp. 434–441.

[16]Winant, C. D., and Browand, F. K., "Vortex Pairing: The Mechanism of Turbulent Mixing-Layer Growth at Moderate Reynolds Number," *Journal of Fluid Mechanics*, Vol. 63, 1974, p. 237.

[17]Ho, C.-M., and Huerre, P., "Perturbed Free Shear Layers," *Annual Review of Fluid Mechanics*, Vol. 16, 1984, pp. 365–424.

[18]Parekh, D. E., Kibens, V., Glezer, A., Wiltse, J. M., and Smith, D. M., "Innovative Jet Flow Control: Mixing Enhancement Experiments," AIAA Paper 96-0308, 1996.

[19]Kibens, V., Dorris, J., III, Smith, D. M., and Mossman, M. F., "Active Flow Control Technology Transition: The Boeing ACE Program," AIAA Paper 99-3507, 1999.

[20]Stanek, M. J., Raman, G., Kibens, V., and Ross, J., "Control of Cavity Resonance Through Very High Frequency Forcing," AIAA Paper 2000-1905, 2000.

[21]Stanek, M. J., Raman, G., Kibens, V., Ross, J. A., Odedra, J., and Peto, J. W., "Suppresison of Cavity Resonance Using High Frequency Forcing: Characteristic Signature of Effective Devices," AIAA Paper 2001-2128, 2001.

[22]Raman, G., and Kibens, V., "Active Flow Control Using Integrated Powered Resonance Tube Actuators," AIAA Paper 2001-3024, 2001.

[23]Hartmann, J., "Construction, Performance, and Design of the Acoustic Air-Jet Generator," *Journal of Scientific Instruments*, Vol. 16, No. 5, 1939, pp. 140–149.

[24]Sarohia, V., and Back, L. H., "Experimental Investigation of Flow and Heating in a Resonance Tube," *Journal of Fluid Mechanics*, Vol. 94, Pt. 4, 1979, pp. 649–672.

[25]Savory, L. E., "Experiments with the Hartmann Acoustic Generator," *Engineering*, Vol. 170, No. 8, 1950, pp. 99, 100, 136–138.

[26]Norum, T. D., and Seiner, J. M., "Broadband Shock Noise from Supersonic Jets," *AIAA Journal*, Vol. 20. No. 1, 1982, pp. 68–73.

[27]Kang, S. W., "Resonance Tubes," Ph.D. Dissertation, Dept. of Mechanical Engineering, Rennsalaer Polytechnic Inst., Troy, NY, Jan. 1964.

[28]Kawahashi, M., and Suzuki, M., "Generative Mechanism of Air Column Oscillation in a Hartmann-Sprenger Tube Excited by an Air Jet Issuing from a Convergent Nozzle," *Journal of Applied Mathematics and Physics (ZAMP)*, Vol. 30, No. 5, 1979, pp. 797–810.

[29]Thompson, P., "Jet-Driven Resonance Tube," *AIAA Journal*, Vol. 2, No. 7, 1964, pp. 1230–1233.

P. J. Morris
Associate Editor